On the interfacial roughness scale in turbulent stratified two-phase flow: 3D numerical simulations with forced turbulence and surfactant

R. Skartlien[a,e,f,*], F. Fakharian[b,a], E. Sollum[c], T. L. Palmer[d]

[a] *FACE - the Multiphase Flow Assurance and Innovation Center, P.O. Box 40, N-2027 Kjeller, Norway*
[b] *Technische Universität München, Germany*
[c] *Norwegian Institute for Air Research (NILU), P.O. Box 100, N-2027 Kjeller, Norway*
[d] *Department of Physics, University of Oslo, P.O. Box 1048, Blindern, N-0316 Oslo, Norway*
[e] *Institute for Energy Technology (IFE), P.O. Box 40, N-2027 Kjeller, Norway*
[f] *Department of Chemical Engineering, NTNU, N-7491 Trondheim, Norway*

Abstract

Numerical simulations of turbulent, stratified two-phase flow with a surfactant laden interface were analyzed. The turbulence was forced in the upper and lower liquids to emulate the dynamics of an interface between turbulent fluids, without requiring (prohibitively) large simulation domains. This setup was used to test and develop a phenomenological roughness scale model where we assume that the energy required to deform the interface (buoyancy, interfacial tension, and viscous work) is proportional to the turbulent kinetic energy adjacent to the interface. The addition of surfactant lead to an increased roughness scale (for the same turbulent kinetic energy) due to the introduction of interfacial dilatational elasticity that suppressed horizontal motion parallel to the interface, and enhanced the vertical motion. We foresee that the phenomenological roughness model can be used as a building block for more general interfacial closure relations in Reynolds averaged turbulence models where also mobile surfactant is accounted for.

*Tel.: +47 63 80 64 67; Fax: +47 63 81 11 68
Email address: roar.skartlien@ife.no (R. Skartlien)

Keywords: Two-phase turbulence modeling, Interfacial closure relations, Surfactant, Interfacial elasticity, Marangoni stress

---

Contents

1. Introduction

The development of a better understanding of turbulence near deformable interfaces has been a long standing research challenge, and experiments and numerical simulations have already revealed many important aspects of the structure of the interface and the adjacent turbulence (e.g., Lugt and Ohring, 1992; Tsai, 1996; Lombardi et al., 1996; Fulgosi et al., 2003; Guo and Chen, 2010). The interfacial fluctuations respond to the turbulent kinetic energy, length scales and vortex structures in the fluids adjacent to the interface (e.g., Rein, 1998; Smolentsev and Miraghaie, 2005) and the turbulence is affected by the interfacial properties (elasticity, viscosity and energy), posing a two-way interface-turbulence coupling. For rigid or stiff interfaces, the turbulence structures resemble those of wall bounded flow, while more flexible interfaces with low energy content are easily deformed by the fluid motions, and the turbulence structures resemble those in the fluid interior, outside boundary layers.

The turbulence-induced interfacial roughness scale in stratified gas/liquid or liquid/liquid flow is an important quantity with respect to the hydrodynamic coupling between the phases. Many two-phase turbulence models for pipe and channel flow rely on interfacial friction models to predict the turbulent (axial) momentum flux transported over the interface from one fluid to the other. In Reynolds averaged models, such as $k-\epsilon$ models, one adopts an interfacial friction model that is often modelled in terms of a roughness scale (e.g., Durbin et al., 2001; Berthelsen and Ytrehus, 2005; Biberg, 2007; de Sampaio et al., 2008), and it is of importance to develop reasonable roughness scale models that can respond to the length, time and energy scales of the turbulence near the interface. Perhaps the most obvious natural system where the roughness scale is central, is the coupling between the ocean surface and the overlying wind (e.g., Charnock, 1955; Wu, 1980; Fernando, 1991). For example, the driving of hurricanes depends on the roughness scale (friction) but also entrainment (heat exchange by sea-spray or droplets) (e.g., Bao et al., 2011).

Earlier, we derived a phenomenological roughness scale model by assuming proportionality between the energy needed to deform the interface and the turbulent kinetic energy adjacent to the interface (Skartlien et al., 2014). This model was tailored to turbulence controlled interfaces with entrainment, and it was tested for gas/liquid pipe flow. The modelled roughness scale could be recast in terms of interfacial capillary, Weber, Froude and

Reynolds numbers, and consistency with models for gravity dominated flows (Charnock, 1955; Wu, 1980) was demonstrated. In the current work, we tested and developed this roughness scale model by using numerical simulations, where all the turbulence length scales and energies near the interface are readily available (within the limitations of the simulation setup). The lattice Boltzmann simulation model we have developed (e.g., Furtado and Skartlien, 2010; Skartlien et al., 2011, and references therein) also includes surfactant, such that we were able to explore how the roughness scale depends on the surfactant dynamics in terms of Marangoni stresses.

Direct numerical simulations of *naturally developed* turbulence with interfaces in two-phase flow is computationally expensive due to the required domain size that is needed to obtain sufficiently large Reynolds numbers (e.g., Menard et al., 2007; Guo and Chen, 2010). In contrast, *forced turbulence* in volumes near the interface allows one to drastically reduce the size of the computational domain while still obtaining sufficiently vigorous turbulence in the interfacial region. However, this offers only an approximate and qualitative way of studying the response and dynamics of the interface to turbulence, since one does not necessarily capture all aspects of the turbulence structures (morphology and size distribution of the vortex structures) that is found in naturally driven two-phase flows. Furthermore, the natural feedback on the turbulence from the interface is not necessarily captured. To prevent a direct forcing of the interface and allow for a naturally developed flow near the interface, "forcing windows" with finite support well outside the interfacial region were invoked. The forcing scheme of ten Cate et al. (2006) for lattice Boltzmann simulations was implemented.

Surfactant lowers the interfacial tension on the average, so that the associated interfacial energy is reduced and the interface may be less stable with larger fluctuation amplitudes, if we assume the same forcing conditions. However, advection of surfactant on the interface in response to the external turbulent flow introduces surfactant density gradients when the interfacial flow is locally divergent/convergent (expanding/contracting). The associated interfacial tension gradients induces tangential Marangoni stresses that oppose the tangential velocities adjacent to the interface (e.g., Sarpkaya, 1996), and this provides a feedback effect that reduces the liquid turbulent kinetic energy near gas/liquid interfaces (e.g., Tsai, 1996; Lee and Saylor, 2010). Much focus has been put on this phenomenon in the context of suppressed surface renewal rates and gas transfer rates over the interface (with emphasis on CO_2 transfer from the atmosphere to the ocean). Tsai (1996)

used numerical simulations to study the effect on the turbulent shear layer under the air-sea interface. The horizontal fluctuations were suppressed, and the vertical fluctuations were also attenuated, in the presence of insoluble surfactant. Lee and Saylor (2010) performed experiments in a wind/water tunnel with a surfactant monolayer, and confirmed that surfactant reduced both the subsurface turbulent fluctuations, and the gas mass transfer rate over the interface.

It must be noted that surfactant may also introduce viscous effects in the interface in addition to elasticity and Marangoni stresses. A more viscous interface acts stabilizing and may suppress capillary waves (the "oil-on-water effect"), while lowered interfacial tension, elasticity and Marangoni effects may act destabilizing on propagating waves (Blyth and Pozrikidis, 2004).

First, we develop a small amplitude version for the interfacial energy model, and this constitutes the the main ingredient in the roughness scale model that we use in the current work. A discussion of the roughness scale model in terms of closure relations in turbulence models, follows thereafter. The 3D simulation setup with the oil/water/surfactant lattice Boltzmann model with forced turbulence is then summarized, before we discuss the roughness scale model in the context of the simulation results.

2. Model for the interfacial energy and roughness scale

An interfacial energy was derived in Skartlien et al. (2014), where we considered interfacial deformations with horizontal scale L (comparable to the turbulent length scale in the fluids parallel to the interface), and height scale δ (the vertical displacement relative to the unperturbed interface in the absence of turbulent kinetic energy). It was assumed that the characteristic fluctuation magnitude was large, so that $\delta \sim L$, and that fragmentation of the interface (entrainment) could occur. In the current work we assume small fluctuations $\delta \ll L$ and no entrainment. There is no fundamental amplitude restriction in the simulation model, but we preferred to study fluctuating interfaces that were not disturbed directly by the turbulence forcing. The forcing was then imposed only beyond a certain distance from the interface, and in this case, our interfaces had small fluctuations.

2.1. Interfacial energy for small fluctuations

A small fluctuation approximation can be obtained by modeling the lifted (or depressed) fluid element by a small cordial segment of a sphere (a spher-

ical cap), of height δ and a circular base area with a diameter equal to the characteristic scale L. This is a suitable model that captures the smoothness of the interface when the fluctuations are small[1]. The excess area relative to the flat interface is now $\Delta A \simeq \pi\delta^2$, and the lifted volume is $\Delta V \simeq (\pi/8)L^2|\delta|$. The center of mass of the lifted element is at $\bar{y} \simeq \delta/3$, and the gravitational potential energy is therefore

$$E_G = (\pi/8)(L^2|\delta|)g\Delta\rho(|\delta|/3), \tag{1}$$

where $\Delta\rho$ is the (positive) density difference between the fluids, and g is the acceleration of gravity. The excess interfacial energy due to interfacial tension σ is

$$E_\sigma = \sigma\Delta A = \pi\sigma\delta^2. \tag{2}$$

The energy spent on viscous dissipation when a fluid element is displaced vertically by an amount $|\delta|$ over the horizontal scale L, is

$$\mu\frac{u_I^*}{L}(\pi L\delta)\delta, \tag{3}$$

expressing the viscous work associated with the internal shearing motion of the fluid inside the lifted volume element (in the "inner fluid"). The characteristic velocity fluctuation of the interface is chosen as

$$u_I^* = \sqrt{(2/3)\bar{k}} \tag{4}$$

where $\bar{k}$ is the average turbulent kinetic energy per unit mass, in the interfacial zone (the averaging is here performed in a horizontal "slab" of sufficient thickness to encompass the interfacial fluctuations).

The viscous resistance in the "outer fluid", that is also displaced, can be significant (displacement into a viscous oil, for example). The associated energy loss can be estimated as a constant factor C_ν times a viscous work term of the same form as that for the inner fluid, so that the total viscous dissipation can be modelled by

$$E_v = (\mu + C_\nu\mu')\frac{u_I^*}{L}(\pi L\delta)\delta \tag{5}$$

[1]The associated sphere has a radius of curvature given by R. The radius of curvature goes to infinity for a flat interface, and limits to $L/2$ for a half sphere with $\delta = R$ as the maximum reasonable excursion.

where μ' is the dynamic viscosity of the outer fluid, and μ is the dynamic viscosity of the inner fluid. With this formulation, we expect that $C_\nu = \mathcal{O}(1)$, and we simply choose $C_\nu = 1$ in the following. The total energy that is needed to displace an interfacial element vertically by an amount δ is therefore

$$E_I = (\pi/8)L^2 g\Delta\rho\delta^2/3 + \pi\sigma\delta^2 + \pi(\mu + C_\nu\mu')u_I^*\delta^2 \equiv F(L)\delta^2. \tag{6}$$

2.2. Roughness scale model

We assume that the interface is fully covered with displaced elements. It is then sufficient to consider the statistics of a single displaced element in order to derive the variance and standard deviation of the fluctuation over the entire interface. The turbulent kinetic energy in the lower fluid serves to displace the elements both upward or downward, and the turbulent kinetic energy in the upper fluid has a similar effect.

We assume that the interface is in local equilibrium with the turbulence, so that the average interfacial energy equals the turbulent kinetic energy that is available to the interface,

$$e_T A_b = \langle E_I \rangle = F(\bar{L})\langle\delta^2\rangle, \tag{7}$$

where angle brackets denote ensemble averaging, $e_I A_b$ is the available energy, e_T is the available energy per unit area, $A_b = (\pi/4)\bar{L}^2$ is the base area of a lifted element, and $\bar{L}$ is an effective interfacial length scale that is induced by the turbulence on both sides of the interface. This defines the model for the roughness scale $\delta^* = \sqrt{\langle\delta^2\rangle}$.

For turbulence-controlled interfacial fluctuations where propagating waves only provide a relatively small contribution, we propose that $\bar{L}$ is approximately equal to an average value between the parallel turbulent length scales in the fluids adjacent to the interface (e.g., Lugt and Ohring, 1992). We will adopt this approximation in the following, and not distinguish the interfacial length scale from the average value of the parallel length scales in the fluids, near the interface. In the following analysis, we will estimate the length scale $\bar{L}$ directly from the velocity field adjacent to the interface, by using the simulation data.

For turbulence modelling purposes, we propose that one could use an *energy averaged* length scale for $\bar{L}$,

$$\bar{L} \;=\; \frac{L_u\rho_u k_u + L_l\rho_l k_l}{\rho_u k_u + \rho_l k_l}, \tag{8}$$

where L_i denotes the parallel turbulent length scale in the fluids. The length scales in either fluid may be taken from the auxiliary turbulence models.

The turbulent kinetic energy adjacent to the interface in fluid i, that is available per interfacial element, is modelled by

$$e_T(i)A_b = \xi \rho_i k_i (d_i A_b)/6, \tag{9}$$

where d_i is the turbulence correlation length perpendicular to the interface, and $\rho_i k_i$ is the turbulent kinetic energy density in fluid i, adjacent to the interface. The physical meaning of this is that the *maximum* amount of energy that is available to lift (or depress) a fluid element of area A_b, is equal to the turbulent kinetic energy contained in the volume $d_i A_b$ adjacent to the interface. This is the volume over which the fluid moves coherently (over the size scale of an eddy). The factor 1/6 is due to the three degrees of freedom of motion, and the fact that the energy can be transported in six directions, among which only one direction involves delivery of energy to the interface. Since the interface is likely to suppress perpendicular motion (due to the "interfacial stiffness"), we introduce a damping factor $1 > \xi > 0$. This damping is discussed below.

The total kinetic energy that is available per displaced element is therefore modelled by

$$e_T A_b = \xi A_b (\rho_l k_l d_l + \rho_u k_u d_u)/6 = \frac{2}{6} \xi A_b \, \overline{\rho k} \bar{d}, \tag{10}$$

by adding the upper and lower contributions. Here, $\overline{\rho k}$ is the arithmetic mean of the upper and lower turbulent kinetic energy densities, and

$$\bar{d} = \frac{\rho_l k_l d_l + \rho_u k_u d_u}{\rho_l k_l + \rho_u k_u}, \tag{11}$$

is the energy averaged perpendicular length scale. From (7) we obtain the following model for the roughness scale δ^*,

$$\delta^* = \sqrt{\frac{(\xi/6)\overline{\rho k}\bar{d}/2}{g\Delta\rho/24 + \sigma/\bar{L}^2 + (\mu_U + \mu_L)u_I^*/\bar{L}^2}}. \tag{12}$$

For relatively weak dissipation and a slow variation of the correlation lengths with turbulent kinetic energy, the roughness scale varies as the square root of the turbulent kinetic energy near the interface. It is also clear that

the roughness scale diminishes for larger density contrast and/or larger interfacial tension and larger viscous dissipation. In the derivation of (12) it was assumed that one half of the elements are upshifted and one half are downshifted, each contributing with a term $(\pi/2)(\mu_U + \mu_L)u_I^*\delta^2$ to the viscous dissipation.

A good fit to the data could only be obtained by choosing a small damping factor of about $\xi = 0.05$. For higher interfacial energy (more rigid interfaces), one may suspect that the damping is larger since the fluid motion is affected more. This results in a smaller effective coherence length close to the interface than what appears to be the size scale d of the most energetic eddies adjacent to the interface (these eddies are illustrated in figure 1). For very stiff interfaces, the coherence length (or mixing length) is proportional to the distance from the interface in accord with the log-law near a solid wall. For low energy interfaces, the fluid is able to move the interface and the coherence lengths are less affected, and for a passive interface that is advected by the flow, there is no damping effect.

2.3. The relation to the volume fraction profile

The ensemble average of the interfacial energy contains the variance $\langle\delta^2\rangle$ of the interface level $h(x, y, t)$, and the corresponding roughness scale $\delta^* = \sqrt{\langle\delta^2\rangle}$ is the standard deviation of the interface level relative to the mean value $\langle h\rangle$. This standard deviation corresponds to the width of an interfacial probability distribution $P(y)$, that relates to the volume fraction profile $\alpha(y)$ over the interfacial zone (Skartlien et al., 2014),

$$\alpha(y) = \int_{-\infty}^{y} P(\zeta)d\zeta. \tag{13}$$

The roughness scale δ^* is then also a measure of the characteristic thickness of the "interfacial zone" over which the volume fraction profile changes between the limiting values (0 and 1).

2.4. Application in turbulence models

By using equation (7), one can normalize the contributions of the interfacial energy terms to the available turbulent kinetic energy, and obtain the non-dimensional form

$$\frac{\langle E_I\rangle}{e_T A_b} = \frac{1}{12}\frac{1}{CFr}\left(\frac{\delta^*}{\bar{d}}\right)^2 + \frac{2}{C}\frac{1}{We}\left(\frac{\delta^*}{\bar{L}}\right)^2 + \frac{2}{C}\frac{1}{Re}\left(\frac{\delta^*}{\bar{L}}\right)^2 = 1, \tag{14}$$

where the interfacial Froude, Weber and Reynolds numbers are defined by

$$\begin{aligned} Fr &= \frac{\overline{\rho k}}{g\Delta\rho\bar{d}}, \\ We &= \frac{\overline{\rho k}\bar{d}}{\sigma}, \\ Re &= \frac{\overline{\rho}u_I^*\bar{d}}{(\mu_U+\mu_L)}, \end{aligned}$$

and where $C = \xi/6$. In equation (14), the term in the Froude number is due to gravitational potential energy, the term in the Weber number is due to interfacial tension, and the term in the Reynolds number is due to viscous dissipation. When any of these non-dimensional numbers are *small*, the corresponding energy term is *large*. The roughness scale (12) can then be recast in terms of these non-dimensional numbers,

$$\delta^* = \frac{\sqrt{12CFr}\ \bar{d}}{\sqrt{1+24(Fr/Re+Fr/We)(\bar{d}/\bar{L})^2}}\ . \tag{15}$$

This model may be used in two-fluid turbulence models that rely on a roughness scale for the prediction of the interfacial stress or interfacial turbulent kinetic energies (e.g., Berthelsen and Ytrehus, 2005; Biberg, 2007). For two-layer $k-\epsilon$ models, Durbin et al. (2001) suggested a quadratic interpolation for the transitional regime between a plane interface where the turbulent kinetic energy is zero ($k=0$), and to the fully rough interface. The corresponding boundary condition for the turbulent kinetic energy above and below the interface took the form

$$k_i = \frac{\tau_I}{\rho_i\sqrt{C_\mu}} Min[1,(R_s^+/90)] \tag{16}$$

with layer index i, and where R_s^+ is a roughness scale, and τ_I is the interfacial shear stress. A specification of R_s^+ is necessary (e.g., via the RMS height of the interface) if the interface is not considered to be "fully turbulent" defined by $(R_s^+/90) > 1$. In this regime, the roughness scale increases with increased turbulent kinetic energy and increased wave heights. Berthelsen and Ytrehus (2005) found that Charnock's gravity controlled length scale (Charnock, 1955) gave reasonable predictions, for gas-liquid flow. The roughness scale model (15) may be used also when viscosity and interfacial tension contributes to the interfacial energy in addition to gravity.

The limiting behavior of (15) is similar to the large amplitude model that was devised in Skartlien et al. (2014). When gravity completely dominates over viscosity and interfacial tension, the characteristic excursion of the interface scales as $\delta^* \simeq \sqrt{12CFr}\ \bar{d}$. The damping constant ξ can be calibrated to match the "Charnock limit" $\delta^* = \beta u_\tau^2/g$, where $\beta \simeq 0.1 - 0.2$ for "shallow water" pipe flow (Berthelsen and Ytrehus, 2005). To be consistent with the roughness scale as it approaches the "fully turbulent" limit, one can consider the interfacial friction velocity in the same limit, $u_\tau^2 \simeq \sqrt{C_\mu}\bar{k} = 0.3\bar{k}$. If we can assume that the roughness scale equals the perpendicular correlation length in this limit, $\delta^* \sim \bar{d}$ (which is reasonable but uncertain), we obtain $\beta \simeq 36C = 6\xi$ from setting $12CFr = 1$, and this yields a value for the damping constant of $\xi \simeq \beta/6$ (with a value of 0.03 for $\beta \simeq 0.2$ – which is close to the fitted value of 0.05 which we use below).

For oil/water combinations with low density contrast, gravity is less important. If, in addition, the Reynolds number is large (small viscous loss), then $\delta^* \sim \sqrt{CWe}\bar{L}$. For very viscous fluids, the Reynolds number is small, and we may have $\delta^* \sim \sqrt{CRe}\bar{L}$ where viscous dissipation limits the interfacial excursions. When the interfacial tension and viscous losses are important, Wu (1980) made a viscous-capillary correction to Charnock's length scale to account for an increased roughness scale due to smaller scale capillary fluctuations. We note that (15) can also account for such viscous-capillary effects.

3. 3D simulations with driven turbulence

3.1. Boundary conditions and simulation setup

The properties of the Shan and Chen type two-fluid lattice Boltzmann model with surfactant were described in earlier work (e.g., Furtado and Skartlien, 2010). A brief summary of the essential ingredients is given in Appendix A. Figure 1 shows the simulation setup with a numerical grid of $100 \times 100 \times 200$ grid points with uniform separation in all three directions. We used $N_y = 200$ grid points in the vertical direction and $N_x = N_z = 100$ in the horizontal directions. Periodic boundary conditions were invoked in both horizontal directions. The upper and lower boundaries were moving no-slip walls to impose a mean shear, and this may affect the interfacial structures and generate a Reynolds shear stress.

The upper and lower fluids were separated by a deformable interface that responded to the flow dynamics (figure 2), and that possessed an interfacial

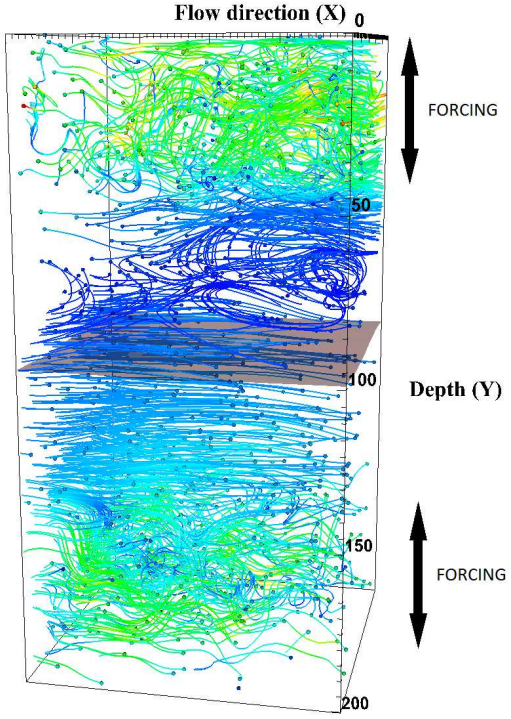

Figure 1: The simulation setup with a numerical grid of $100 \times 100 \times 200$ grid points. The interface between the upper fluid (less viscous), and the lower fluid (more viscous) is shown in grey. Streamlines visualize the instantaneous velocity field, with a color coding that depends on the velocity magnitude. Green/yellow indicates larger velocities than blue. The small dots at the end of the streamlines mark the starting point of the integration. The upper and lower walls were moving to impose a mean shear, and the lower fluid moves to the left on the average.

tension that was reduced by the presence of surfactant. The upper fluid had a smaller density than the lower fluid, making the setup Rayleigh-Taylor stable against gravity. The lower, more dense fluid had the higher viscosity in the current setup. This was more numerically stable in our lattice-Boltzmann implementation. We note that a light-oil and water case implies oil as the upper more viscous fluid, in contrast to our case. The density ratio and hence the buoyancy of the fluids were controlled by van der Waals like self-interaction forces via the force parameters $\mathcal{G}_{AA}$ or $\mathcal{G}_{BB}$ as described in Appendix A. We chose a moderate density ratio of 2, and a kinematic viscosity ratio of 2.5. The collisional relaxation times in lattice Boltzmann model that determine

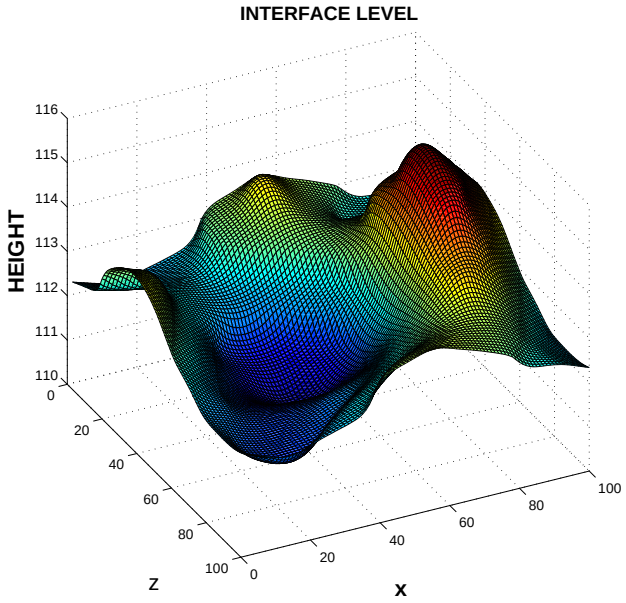

Figure 2: Interfacial fluctuations at a specific time.

the kinematic fluid viscosities, were $\tau_w = 1.1$ and $\tau_o = 2.0$ for the water and oil phases respectively, providing the given viscosity ratio.

The simulations were started by imposing a piecewise linear velocity profile $u_x^0(y)$ that matched the moving wall velocities, while obeying a constant viscous stress $\tau_v = \mu \partial_y u_x^0$ throughout the domain. The averaged streamwise velocity V_x display a similar profile (figure 3), where the viscous stress dominates and controls the slopes of the velocity profile. The Reynolds shear stress was found to be marginal compared to the viscous stress. The mean shear rate $\partial_y V_x$ implies a turnover or circulation frequency of about 30 s^{-1}, with the lattice Boltzmann normalization parameters we chose (Appendix B).

The surfactant is soluble in both fluids, and the mass density of the surfactant (mass per unit volume) relative to the water density was 1.5×10^{-2} in the bulk phases. The surfactant forces were turned off for the "surfactant free case" where the interfacial tension had a constant and high value of 15 mN/m with the chosen normalization parameters. Under static conditions, the surfactant adsorbs to the interface in the lattice Boltzmann model until an equilibrium is achieved with the bulk concentration (Skartlien et

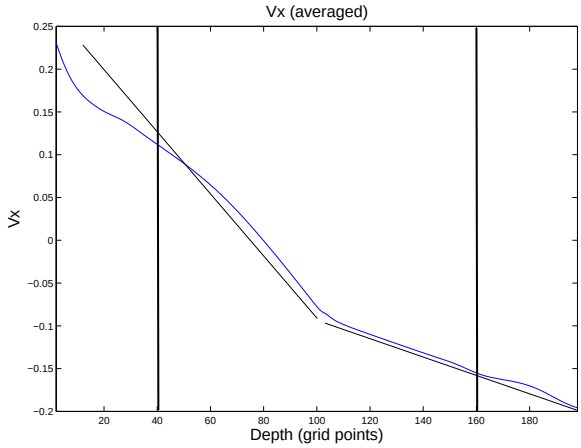

Figure 3: The average streamwise velocity $V_x(y)$. The different slopes are a consequence of the viscous stress, and the response to the different fluid viscosities. The straight lines illustrate the velocity profile that corresponds to a constant viscous stress and the given viscosity contrast. The boundaries of the upper and lower volumes where the turbulent forcing was imposed, are shown by vertical lines.

al., 2011), and the interfacial tension was reduced by about 25%, with force parameters given in Appendix A.

3.2. Driven turbulence and parallel processing

Forced turbulence was applied as a means of obtaining sufficient turbulent kinetic energy to drive the interface without having to realize a large Reynolds number that requires a much larger simulation domain. In this way, we avoided the very large computational loads as noted in the introduction, but at the cost of only approximate turbulence structures. A stochastic force was applied in the upper and lower fluids (figure 1), within zones that extended from the upper and lower moving walls and to a distance of 50 grid points above and below the interface as indicated in the figure. The stochastic force was scaled down linearly towards the interface over a narrow zone (10 grid points), and there was no forcing closer than 50 grid points of the interface. One half of the simulation volume (centered at the interface) was then forcing-free, in which the turbulence could evolve freely.

The stochastic force was defined in spectral space, with a low wave number, narrow band isotropic power spectrum, as described in Appendix C. The power spectrum was defined on a spherical shell with a radius or central

wavenumber k_f, and a with a relatively narrow bandwidth Δk. The energy input rate provided by the driving force is given by $\epsilon = (u^*)^3/\bar{l^*}$ (ten Cate et al., 2006), where $\bar{l^*}$ can be taken as the average driving wavelength which is proportional to $1/k_f$. Several values of the energy input rate were used by varying u^* between 0.05 and 0.4. The energy input rate, and therefore the interfacial fluctuations, were kept sufficiently small to avoid large interfacial undulations and direct forcing of the interface in the upper and lower forcing volumes. A characteristic turbulent velocity parameter of $u^* = 0.1$ corresponds to a turbulent RMS velocity of 0.14 m/s (with the chosen normalization parameters in Appendix B).

A total of 18 simulations without surfactant and 9 with surfactant were carried out. A large number of time steps (30000) were necessary in each case, to suppress the statistical noise (or uncertainty) in the averaged simulation data. The total computational time was about 25 days on 12 microprocessors run in parallel. MPI was used to parallelize the code, by splitting the domain in equal size slabs in the flow direction (x-direction). The discretized populations of the Boltzmann distribution that move across the corresponding boundaries were communicated between the microprocessors.

4. Results

First, we describe the flow morphology and resulting lengths scales that emerge in the simulations, before we discuss the results in the context of the roughness scale model.

4.1. Length scale estimates from the simulations

The average turbulent kinetic energy $\overline{\rho k}$ in the interfacial zone (defined as a 3D slab of vertical thickness equal to 20 grid points, that contained the fluctuating interface) increased with the energy input rate ϵ. Figure 4 shows that $\overline{\rho k}$ increased roughly linearly with ϵ. The turbulent kinetic energy profile as function of height, decreased exponentially from the forcing volumes and towards the interface (figure 5). These profiles are approximately proportional to ϵ, giving the variation in the average turbulent kinetic energy in the interfacial zone, as shown in figure 4.

The turbulent length scales parallel and perpendicular to the interface in the regions between the forcing volumes and the interface, were estimated by visualizing the most energetic eddies using instantaneous streamlines, and by using autocorrelation functions of the velocity field. Figure 6 (and figure 1)

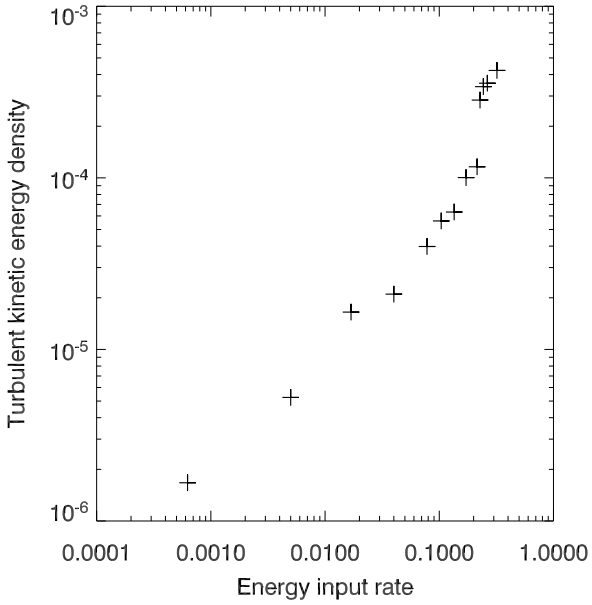

Figure 4: The average turbulent kinetic energy $\overline{\rho k}$ adjacent to the interface as function of the input rate ϵ of turbulent kinetic energy in the forcing volumes.

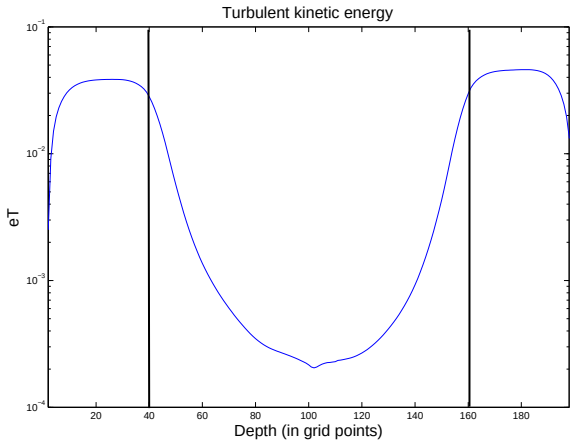

Figure 5: A profile of the turbulent kinetic energy $\overline{\rho k}$ as function of distance between the walls. The boundaries of the forcing volume are shown by vertical lines, and the turbulent kinetic energy decayed towards the interfacial region in the middle of the domain.

show streamline visualizations, and figure 7 shows some of the autocorrelation lengths that were calculated. The correlation lengths were consistent with the eddy-size estimates, and they did not show a clear decreasing trend with increasing energy input rate ϵ. We obtained $\bar{d} \simeq \bar{L}/2 \simeq 32$ as an estimate that could represent all the cases.

The eddy length scale was in general larger than the average forcing length scale of $l_x^* = 20$. The reason for this, and the almost constant length scale with increasing energy input, is that the characteristic eddy size was strongly influenced by the applied shear. The turbulent velocities induced by the forcing, and the velocity components induced by the shear, were in fact equally important; the velocity increment $(\partial_y V_x)\Delta y$ over the distance Δy between the boundary of the forcing volume and the interface was of similar magnitude as the characteristic turbulent velocity $u^* = \mathcal{O}(0.1)$.

It was confirmed that the eddy size was not sensitive to the horizontal extent of the simulation domain, as shown in the right hand panel in figure 6. The domain size in the flow direction (streamwise direction) was increased by a factor of two. This indicates that the eddy size was mainly controlled by the distance Δy between the boundary of the forcing volume and the interface. Furthermore, for *non-moving* upper and lower walls, the characteristic regular pattern of the larger eddies vanished, leaving only smaller and more randomly distributed eddies.

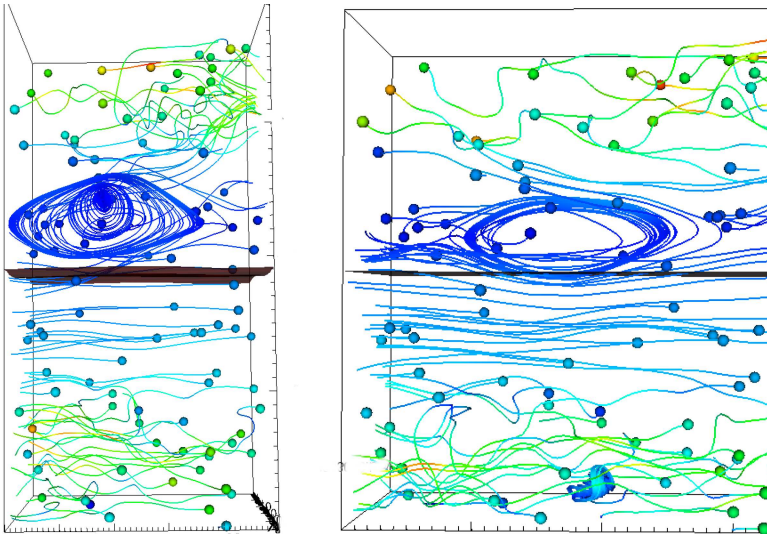

Figure 6: Streamline visualization was used to estimate the eddy sizes (the streamline coding is the same as in figure 1. Only the eddies above the interface is visible, since the streamwise velocity component fluctuates around zero only in this region. The left panel shows a characteristic eddy for a domain size of 100 grid points in the streamwise direction, and the right hand panel shows that the characteristic eddy size did not change appreciably even with 200 grid points in the streamwise direction.

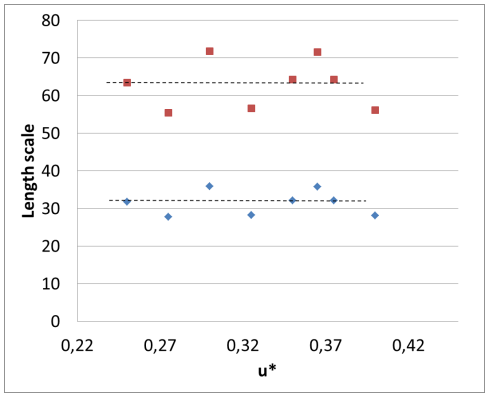

Figure 7: The length scales were also estimated by using correlation functions of the velocity field. The figure shows the corresponding $\bar{d}$ (diamonds, smaller values) and $\bar{L}$ (squares, larger values). The dashed lines mark the average values, and these were consistent with visual eddy-size measurements using streamlines. We obtained $\bar{d} \simeq \bar{L}/2$ for all the cases, indicating that the sizes of the larger, more energetic eddies were strongly influenced by the mean shear.

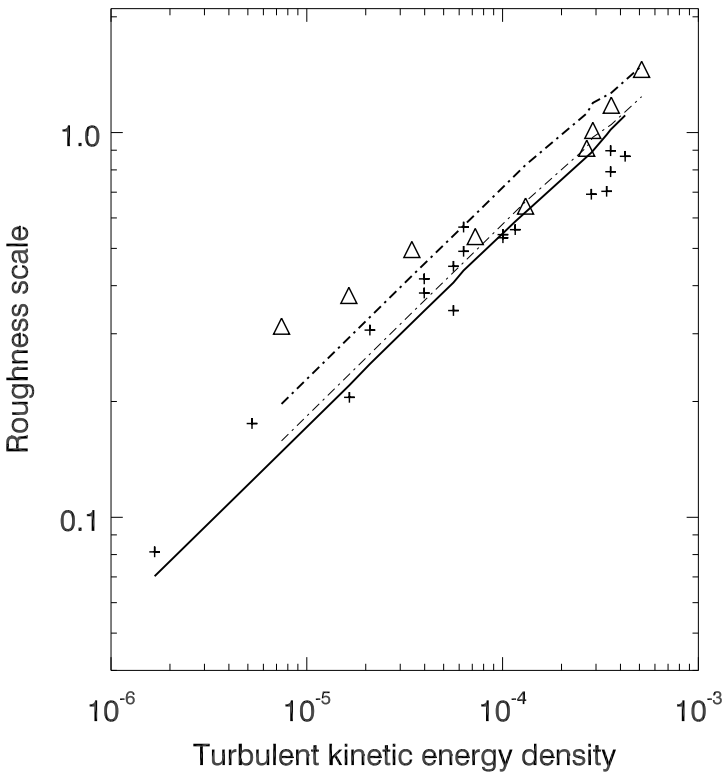

Figure 8: The estimate of the interfacial roughness scale δ^* in the simulation data without surfactant (crosses), and with surfactant (triangles) as function of the turbulent kinetic energy $\overline{\rho k}$ in the interfacial zone. This log-log plot reveals the square root dependency of the roughness scale as function of turbulent kinetic energy, as predicted from the phenomenological roughness scale model. The thick full line shows the model result without surfactant. With surfactant, the simulation data show an interfacial roughness that is overall larger than expected: The thick dash-dot line shows the model result with zero interfacial tension. The average surfactant density corresponds to a reduction of the interfacial tension only by about 25% relative to the surfactant free case, and the thin dash-dot line shows the corresponding model result.

4.2. Roughness scale: model versus simulations

The roughness scale δ^* was estimated from the simulation data, as the standard deviation of the fluctuating interface level over all time steps after an initial period that contained startup transients. Figure 8 shows the estimated δ^* as function of the average turbulent kinetic energy $\overline{\rho k}$. The roughness scale with surfactant (triangles) was overall larger than for the "clean" surfactant-free case (crosses). Even though the noise component in these estimates is significant, we confirm a square root dependency of the roughness scale as function of turbulent kinetic energy (straight lines). This is predicted by the model in the limit of relatively small viscous dissipation.

The thick full line shows the surfactant free model result, using the interfacial tension from the simulation model, and the model fit the data (crosses) well when the damping factor was tuned to $\xi = 0.05$. The length scales ($\overline{L}$ and $\overline{d}$) are input parameters to the model, and these were taken from the simulation data ($\bar{d} \simeq \bar{L}/2 \simeq 32$ from figure 7).

Surfactant lowers the interfacial energy on the average, and based on this alone, one should expect that the roughness should increase, provided that the turbulent kinetic energy is the same. The average surfactant density corresponds to a reduction of the interfacial tension by about 25% relative to the surfactant free case. When this reduced interfacial tension was used in the model, only a relatively small increase in the roughness scale was obtained as shown by the thin dash-dot line. The thick dash-dot line shows an upper limit estimate from the model by setting the interfacial tension to *zero*, and this seems to represent a better fit to the data (triangles). The interfacial roughness with surfactant was therefore larger than what can be obtained by a simple reduction of the average interfacial tension.

We propose that the transversal (vertical) velocity fluctuations (these are responsible for the roughness scale) increase when the tangential (horizontal) velocity fluctuations are suppressed by the Marangoni stresses, as a consequence of momentum balance and mass conservation near the interface. This is expected if one imposes the same forcing conditions on the interface (the same turbulent kinetic energy) also in the presence of surfactant. We analyze this in more detail in section 5.2.

4.3. Interfacial energy contributions

The normalized interfacial energy contributions is given by equation (14). Each term is proportional to the inverse Froude, Weber and Reynolds numbers, defined via the relatively small depth scale $\bar{d}$ near the interface (this

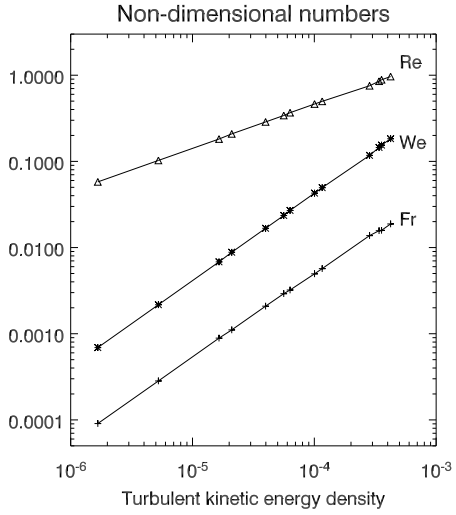

Figure 9: Non-dimensional numbers for the interface as function of average turbulent kinetic energy density $\overline{\rho k}$ in the interfacial zone. The Froude number was the smallest, meaning that gravitational potential energy was the most important interfacial energy term in the current setting.

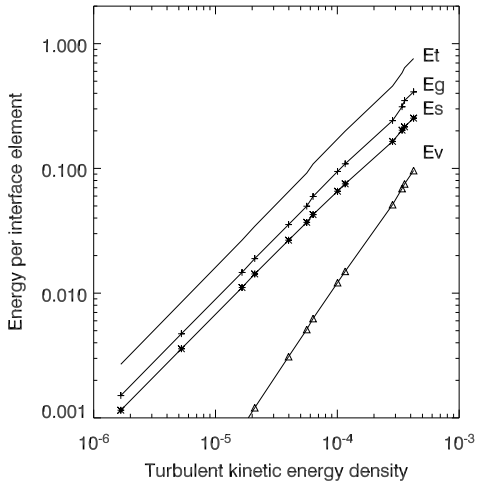

Figure 10: The interfacial energy contributions as function of $\overline{\rho k}$. The full line shows the total energy E_t. E_g is the gravitational potential energy, E_s is the interfacial tension term, and E_v is the viscous dissipation term.

generates small interfacial Reynolds numbers, even though the usual flow Reynolds number can be large). These non-dimensional numbers are shown in figure 9 as function of turbulent kinetic energy. The Froude number was the smallest, and the Reynolds number was the largest, meaning that gravitational potential energy was the dominating interfacial energy term, and that viscous dissipation was a small contribution. The interfacial tension provided an intermediate energy term, via the Weber number.

The ensemble averaged interfacial energy terms in equation (6), with L substituted by the energy averaged $\overline{L}$ from equation (8), are shown in figure 10. The thick full line shows the total energy (which is set equal to the available turbulent kinetic energy in the roughness scale model). All terms increase with turbulent kinetic energy mainly due to the increasing interfacial fluctuation $\langle \delta^2 \rangle$, but the viscous dissipation term increases more rapidly since it is also directly proportional to the fluctuation velocity u_I^* at the interface.

5. Influence of the dilatational elasticity

5.1. Interfacial surfactant distribution and flow fields

The surfactant was not evenly distributed on the interface, as shown in figure 11. The surfactant density was about 0.02 in the bulk, and it fluctuated between 0.03 and 0.05 on the interface. Consequently, the interfacial tension fluctuated by about 15%, and this induced tangential stresses that varied across the interface. If the interfacial flow expands locally due to nearby turbulent flow (internal to the fluids), an opposing Marangoni stress is induced that tends to oppose this expansion, and this corresponds to a dilatational elasticity (e.g., Danov et al., 2001).

The length scale of the fluctuations in surfactant density on the interface was comparable to the characteristic eddy size scale as seen in figure 11. There was also a correlation between upward interfacial fluctuation into the less dense/less viscous upper fluid and lowered surfactant density (the round, lighter patches in the figure). The reason for this is that a local expansion of the interface dilutes the surfactant density locally, when there is an upwelling in the more viscous fluid towards the interface. The more viscous fluid controlled this interfacial flow field, since the velocity gradients adjacent to the interface were of similar magnitude in the upper and lower fluids and the interfacial viscous stress $\tau_v = \mu \partial_y u_x$ is then larger when the motion is induced by the more viscous fluid. The surfactant density was larger in interfacial regions where the flow was converging, in between the expanding

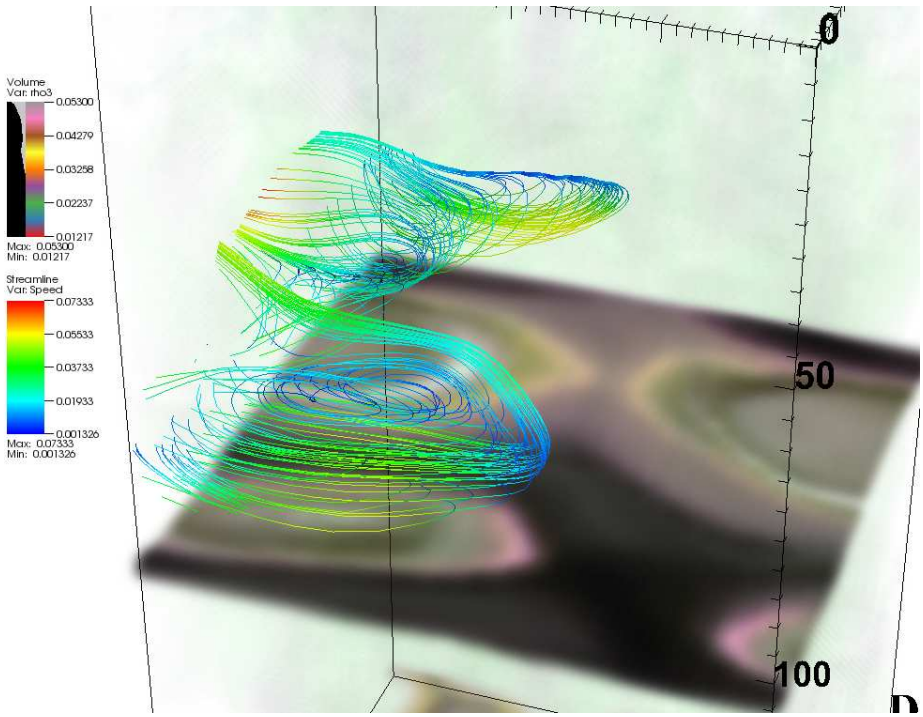

Figure 11: The surfactant density varied along the interface with a characteristic length scale that was comparable to the size of the most energetic eddies (visualized by the streamlines). Dark shades on the interface mark elevated surfactant concentrations, and pink/yellow renders lower surfactant concentrations. The surfactant was soluble in both phases, and the bulk concentrations are seen as a green "haze".

patches. This is also where the interface was depressed into the more viscous fluid.

5.2. Pressure fluctuations induced by dilatational elasticity

If the surfactant is sufficiently mobile (implying unsaturated interfaces), gradients in the interfacial surfactant concentration will be induced in response to the external flow. The corresponding Marangoni stress is (e.g., Danov et al., 2001)

$$\tau_M = \partial_s \sigma, \tag{17}$$

where the interfacial tension σ is reduced for increasing interfacial surfactant density Γ, and $\partial_s(..)$ signifies the derivative along the interface.

In the following analysis we assume a constant level of turbulent kinetic energy near the interface (with and without surfactant), and impose a constant localized mass flux towards the interface (from below) through the area $A_b \simeq L^2$, and calculate the resulting change of the interfacial lift when the Marangoni stress is added. The mass flux is diverted horizontally and parallel to the interface (in an axis-symmetric fashion with a stagnation point somewhere on the symmetry axis) and there is no mass flux through the interface. The mass flux parallel to the interface is therefore equal to the flux towards the interface. For an order of magnitude estimate, we assume a simple 2D geometry and a steady flow (vanishing time derivatives). The average fluid velocity parallel to the interface is then given by

$$\rho(\partial_y(\overline{u_x^2}/2)) = -\partial_y P + \frac{1}{h}(\tau_M + \tau_v), \tag{18}$$

where h is a characteristic "penetration depth" of the flow (the boundary layer thickness of the horizontal flow), x is the coordinate along the interface, $\overline{u_x^2}$ and $P(x)$ are the squared velocity and pressure averaged over the depth h (starting at the interface), and τ_v is the viscous stress at the interface. Both the velocity and the pressure vary with x, and the pressure decreases away from the symmetry plane (in both directions). We have assumed that the scale of variation of $u_x(x)$ is much larger than h, so that the viscous stress term can be simplified.

The viscous stress at the interface is a source of interfacial flow that generates a Marangoni stress τ_M that opposes the pressure gradient that drives the diverging flow. Since we impose the same mass flux both with and without surfactant, $\overline{u_x^2}$ is not altered, and the pressure below the interface

must increase locally to drive the same mass flux. Consequently, the interface is lifted more in order to balance the increased pressure difference between the upper and lower fluids. The change in pressure in the lower fluid is, by (18),

$$\Delta P \simeq \frac{L}{h}|\tau_M| \tag{19}$$

and the magnitude of the lift can be estimated by equating the increased energy $(\Delta P)V$ in the characteristic volume $V = L^2 h$, with the increased interfacial energy ΔE_I of the lifted element,

$$(\Delta P)V = \Delta E_I = F(L)(\Delta\delta^2). \tag{20}$$

The Marangoni stress is

$$\tau_M = \partial_s \sigma = (\partial_s \Gamma)(\partial_\Gamma \sigma) \simeq -\frac{E_G}{L}\frac{\Delta\Gamma}{\Gamma}, \tag{21}$$

where $E_G = -\Gamma\partial_\Gamma\sigma$ is Gibbs elasticity. One then obtains an increment in the variance of the interfacial level that scales as

$$\Delta\langle\delta^2\rangle \sim L^2 \left\{ \frac{E_G}{F(L)} \left\langle \frac{|\Delta\Gamma|}{\Gamma} \right\rangle \right\}. \tag{22}$$

In the current simulations, we may take $E_G \simeq \Delta\sigma$ (as explained in Appendix D). F is an interfacial energy per unit area, and the non-dimensional number E_G/F measures the importance of the elasticity, relative to the total interfacial energy that is associated to the length scale L. $\Delta\Gamma/\Gamma$ can be taken as the fluctuation of the interfacial surfactant density relative to the average value on the interface. These fluctuations increase with turbulent kinetic energy due to increased fluctuations in tangential viscous stresses.

To estimate the order of magnitude of the increase in the roughness scale, we adopted characteristic input parameters from the simulations. We found $E_G/F \simeq 0.01/0.5 = 0.05$, and based on the measured maximum and minimum values of the interfacial surfactant concentration, we found $|\Delta\Gamma|/\Gamma \simeq 0.02/0.04 = 0.5$. The corresponding estimate of the increase of the roughness scale is then $\Delta\delta^* \sim 0.1\bar{L} = \mathcal{O}(1)$, which is relatively large. The measured standard deviation indicates a more moderate increase on the order of 0.1 units.

6. Discussion

The large amplitude model for the interfacial energy that we devised previously (Skartlien et al., 2014), did not yield results that compared well with the simulation results, because the energy contribution from the interfacial tension was overestimated. A spherical cap geometry to capture the smoothness of small amplitude interfacial fluctuations was therefore introduced (rather than the cylindrical geometry for large amplitude, stretched fluid filaments). A damping constant had to be invoked to account for a reduction of the turbulent kinetic energy towards the interface. The tuned value of the damping constant was consistent with the Charnock constant for fully turbulent interfaces. The damping is expected to vary with turbulent kinetic energy, being larger for more stiff interfaces, and a fully self contained model should account for this effect.

In more realistic turbulence that develops from wall boundary layers (rather than the forced turbulence we invoked), one expects that the correlation lengths near the interface decreases significantly with turbulent kinetic energy (in our case these correlation lengths did not vary much with turbulent kinetic energy, due to the eddies that were induced mainly by the applied mean shear). This would increase the capillary energy (the interfacial tension contribution) and the viscous dissipation relative to the gravitational potential energy, when the turbulent kinetic energy increases. These dependencies could result in a significant reduction of the roughness scale for higher turbulent kinetic energies, relative to the square root dependency we found.

When surfactant is added, one can in general expect both elastic and viscous effects in the interface. The extra interfacial viscosity was negligible in the simulations due to a very small surfactant density, and interfacial shear elasticity was not accounted for. However, dilatational elasticity (Marangoni stresses) was accounted for via the variation of interfacial tension with local interfacial surfactant density.

In naturally driven turbulence (such as wind driven turbulence) it is known that the addition of surfactant tends to suppress the turbulent kinetic energy near the interface due to Marangoni stresses, given the same external driving conditions (such as a given wind speed or a given pressure drop along a pipe). This is a common effect below air water interfaces (e.g., Lee and Saylor, 2010), where also the vertical velocity fluctuations are suppressed (e.g., Tsai, 1996). This implies a less rough interface in the vertical direction, in contrast to our current findings where the vertical roughness

scale increased. The reason for this discrepancy is that the forcing in the simulations determined the turbulence levels adjacent to the interface, so that the natural feedback (turbulence damping) from the Marangoni stresses was not captured. Our model equations for the roughness scale can however be applied directly with a reduced turbulent kinetic energy to allow for the feedback effect.

Equation (20) suggests that the increased pressure perturbations near the interface due to the opposing Marangoni stresses could be modelled by

$$\langle \Delta P \rangle V = \eta \frac{L}{h} \langle |\tau_M| \rangle (L^2 h) = \eta L^2 E_G \left\langle \frac{|\Delta\Gamma|}{\Gamma} \right\rangle, \tag{23}$$

and this could be added to the turbulent kinetic energy given by (10) to account for the amplification of the roughness scale. The factor η is expected to be less than unity (implied by the estimates in section 5.2). The "missing link" in this description is a relation between fluctuations in $\Delta\Gamma$ and the turbulent kinetic energy near the interface. This would involve a model for the turbulent viscous stresses at the interface, and a model for the flow of surfactant on the interface that incorporates advection and diffusion.

7. Conclusion

Simulations with forced turbulence allowed for a study of interfaces in turbulent flow without the need for very large simulation domains and large Reynolds numbers. This setup offered only approximate turbulent conditions, but it proved to be a useful "test bench" to study the assumptions and ingredients in the roughness scale model, also in the presence of soluble and mobile surfactant.

The phenomenological model for the interfacial roughness scale represented the simulation results quite well in terms of a reasonable scaling with varying turbulent kinetic energy. The model can, in its current form, be used as a closure relation in two-phase turbulence models for stratified flow without surfactant, provided that one can predict the damping of turbulent kinetic energy towards the interface. Gravitational potential energy, interfacial tension and viscous deformation work were accounted for, and the model should therefore be reasonable for both oil/water and liguid/gas flows.

Larger interfacial fluctuations were observed in the simulations when surfactant was added (given the same level of turbulent kinetic energy adjacent

to the interface), due to dilatational elasticity (Marangoni stress) that opposes tangentially divergent and convergent flow fields adjacent to the interface. A lowered average interfacial tension parameter can not account for this effect.

The roughness scale model was not fully developed for dilatational elasticity in this work, but we proposed a source term for pressure fluctuations near the interface, that can be added to the turbulent kinetic energy density that would occur in the absence of surfactant. This source term should be developed further so that the surfactant density fluctuations in the interface can be related to the turbulence adjacent to the interface. With these developments, we expect that a complete roughness scale model with surfactant can be developed.

Appendix A. Three-component (oil/water/surfactant) lattice Boltzmann force model

The model surfactant is soluble in both fluids, representing an ampliphilic surfactant structure with an organic tail and a polar head. The surfactant is treated as continuous fluid with a vector associated to it, representing the average direction of the surfactant molecules in the local computational cell. This vector field evolves in time in response to the dynamic interfaces.

A detailed description of the Shan and Chen type lattice Boltzmann model used in this work was given in earlier work (e.g., Furtado and Skartlien, 2010). The simple non-ionic surfactant model that uses two connected unlike "particles", A and B, representing hydrophilic and hydrophobic parts of a surfactant molecule, S=A+B. The two ordinary fluids are assumed to be composed of particles similar to the A and B components of the surfactant, producing an A-fluid and a B-fluid representing oil and water. The force between any two pairs of "particles" has the form

$$\mathfrak{F}_\alpha = \pm \frac{\mathcal{G}}{C^D} C_\alpha, \tag{A.1}$$

where $C = |\mathbf{C}| = |\mathbf{R}_j - \mathbf{R}_i|$, is the inter-particle separation, and where $D = 3$ is the number of spatial dimensions (3 in this work). The coupling constant is chosen so that that like particles attract while unlike ones repel, and this provides immiscibility between the fluids, A and B, and an affinity of the surfactant with the interface between the fluids.

This basic force model give rise to a number of coupling constants: $\mathcal{G}_{AB}$ for interactions between fluids, $\mathcal{G}_{AA}$, $\mathcal{G}_{BB}$ for interactions between particles of the same kind, $\mathcal{G}_{AS}$ and $\mathcal{G}_{BS}$ for fluid-surfactant interactions, and $\mathcal{G}_{SS}$ for surfactant-surfactant interactions. The self interaction parameter of the more dense fluid $\mathcal{G}_{BB}$ (here, oil) is negative to provide a denser fluid for the same pressure, inducing gravitational stabilization of the interface.

The model surfactant exhibits diffusion controlled adsorption kinetics (Skartlien et al., 2011), where the surfactant adsorbs to the interface from

$\mathcal{G}_{AA}$	$\mathcal{G}_{BB}$	$\mathcal{G}_{AB}$	$\mathcal{G}_{AS}$	$\mathcal{G}_{BS}$	$\mathcal{G}_{SS}$
0.0	-2	3	-2	2	0.13

Table A.1: Interaction coupling constants. The signs chosen for these constants are a consequence of the formulation of the force model (Furtado and Skartlien, 2010).

the bulk phases over a characteristic timescale. The solubility in either fluid can to some extent be adjusted via the force parameters. The force parameters that were used in the current work are given in Table A.1, and these give comparable solubilities in the fluids, and a significant reduction of interfacial tension due to the surfactant. The equilibrium interfacial tension was reduced by about 25% relative to the interfacial tension in a surfactant free system. The dynamics in the fluids induce fluctuations in the interfacial surfactant density and Marangoni effects (via the viscous stresses) and no explicit advection/diffusion equation for the surfactant on the interface is necessary. The diffusivity of the surfactant is controlled by the kinematic viscosities of the fluids and of the surfactant fluid (Skartlien et al., 2011). We chose a collisional relaxation time $\tau_S = 1.1$ for the surfactant, defining the kinematic viscosity of the surfactant, as a fluid. The rotational relaxation time of the amphiphile was set to $\tau_d = 5.0$, and the surfactant temperature parameter was set to $T_s = 0.1$.

Appendix B. Normalization and scaling

In lattice Boltzmann models, all the physical quantities are normalized to the length, time, and mass scales given by the grid separation Δx, timestep Δt, and the chosen mass density ρ_c. To obtain physical units, one can scale the simulation results with the values of these primary normalization constants. For the choice $\Delta x = 0.1\ mm$, $\Delta t = 70\ \mu s$ and $\rho_c = 1000\ kg/m^3$, the domain size is $1 \times 1 \times 2\ cm$, and the interfacial tension becomes $15\ mN/m$, characteristic for an oil/water interfacial tension (the interfacial tension is also dependent on the interaction forces and the coupling constant $\mathcal{G}_{AB}$ as described in Appendix A). The gravitational constant is now 6×10^{-4}, which corresponds to a low gravitational acceleration of $0.02\ m/s^2$.

Appendix C. Spectral forcing

A low wave number, narrow band driving force $\mathbf{F}$ provided the same acceleration to both fluids (including the surfactant). The isotropic power spectrum of each force component i, was defined on a spherical shell of the form (ten Cate et al., 2006)

$$F_i(k) = A \exp\left(\frac{(k - k_f)^2}{\Delta k^2}\right). \tag{C.1}$$

The central wavenumber is k_f and the bandwidth is Δk. For single phase flow, it has been shown that when k_f is located in the lower inertial subrange, a turbulent cascade proceeds down to the Kolmogorov scale (ten Cate et al., 2006). A divergence free force ($\nabla \cdot \mathbf{F} = 0$ in physical space) was enforced to limit compression/expansion and sound waves (the LBM fluid is compressible by nature of the method). We note that by scaling the forcing with a spatially varying function, one invalidates the divergence free forcing condition and some sound waves were therefore generated in the narrow zones where the force was scaled down.

The energy input rate is proportional to the RMS of the force fluctuations and a work term of the form $\mathbf{F} \cdot \mathbf{V}$, where $\mathbf{V}$ is the local fluid velocity. The method of Alvelius (1999) was adopted that provides $\mathbf{F} \cdot \mathbf{V} = 0$ at every timestep, to prevent an increase of energy in the system over time, and the energy input rate is then only dependent on the variance (or total power) of the driving force.

The input parameters for the forced turbulence is the characteristic turbulent velocity u^*, and the central wavelength of the driving force, $l_i^* = N_i/k_f$, where N_i is the number of grid points over the domain in direction i. The energy input rate provided by the driving force is given by $\epsilon = (u^*)^3/\bar{l^*}$ (ten Cate et al., 2006), where $\bar{l^*}$ can be taken as the average driving wavelength. We used the same turbulence driving force statistics (length and velocity scale parameters) in both fluids and we chose a driving wavenumber of $k_f = 5$ in all three directions (meaning 5 wavelengths over the extent of the domain in all directions), and we chose a bandwidth of $\Delta k = 4$. The characteristic eddy size in the forcing volumes was comparable to $l_x^* = N_x/k_f = 20$ grid points.

Appendix D. Interfacial elasticity

The Langmuir interfacial tension isotherm

$$\sigma = \sigma_0 + RT\Gamma_m \ln(1 - \Gamma/\Gamma_m), \tag{D.1}$$

is a good representation of the current simulation model as shown in Skartlien et al. (2011), where σ is the interfacial tension, σ_0 is the surfactant-free interfacial tension, Γ_m is the maximum interfacial concentration, T is the temperature, and R is the "gas constant". Gibbs elasticity (e.g., Danov et al., 2001) is then

$$E_G = \frac{RT\Gamma}{1 - \Gamma/\Gamma_m}. \tag{D.2}$$

For the current work, $\Gamma/\Gamma_m \ll 1$, so that we may take $E_G \simeq RT\Gamma$ to first order. To the same order, we may take $\Delta\sigma = \sigma_0 - \sigma \simeq RT\Gamma$, so that

$$E_G \simeq \Delta\sigma. \tag{D.3}$$

Appendix E. Interfacial energy terms for large fluctuations

A different roughness scale model results for the large amplitude fluctuations (Skartlien et al., 2014), where the interfacial tension becomes more important relative to gravity and dissipation. If one assumes a base area of $A_b = \pi L^2/4$, and a finite amplitude, cylindrical geometry to represent stretched liquid filaments, one obtains an interfacial energy per displaced element of (Fakharian, 2013; Skartlien et al., 2014)

$$E_I = (\pi/4)(L^2|\delta|)g\Delta\rho(|\delta|/2) + \pi\sigma L|\delta| + \pi(\mu + C_\nu\mu')u_I^*\delta^2, \tag{E.1}$$

where the interfacial tension term is of first order in the displacement δ, in contrast to the current small amplitude model, where all terms are of second order in the displacement. The roughness scale is now given by a second order algebraic relation that can be recast in terms of the three non-dimensional numbers,

$$\left[\frac{1}{Fr}\frac{1}{8\bar{d}^2} + \frac{1}{Re}\frac{2}{\bar{L}^2}\right](\delta^*)^2 + \left[\frac{1}{We}\frac{2}{\bar{L}}\right]\delta^* - 1 = 0. \tag{E.2}$$

When gravity is dominates over viscosity and interfacial tension, the characteristic excursion of the interface scales as $\delta^* \sim \sqrt{Fr}\bar{d}$, as for the low amplitude model. One obtains $\delta^* \sim We\bar{L}$ for large Reynolds numbers and low density contrast, and $\delta^* \sim \sqrt{Re}\bar{L}$ for a viscosity dominated regime.

Acknowledgements

We acknowledge the financial support from The Multiphase Flow Assurance and Innovation Centre (FACE), a research cooperation between IFE, NTNU and SINTEF, funded by The Research Council of Norway and by the following industrial partners: Statoil ASA, GE Oil & Gas, SPT Group, FMC Technologies, CD-adapco, Shell Technology Norway. The work relied heavily on the following freeware: The Unix emulator Cygwin, MPICH (an implementation of the Message Passing Interface for parallell processing), the 3D visualization tool Visit, Ghostview, and the graphics tool Gimps.

References

Alvelius, K., 1999. Random forcing of three-dimensional homogeneous turbulence. Physics of Fluids 11, 7, 1880-1889.

Bao, J.-W., Fairall, C. W. , Michelson, S. A., Bianco, L, 2011. Parameterizations of Sea–Spray Impact on the Air-Sea Momentum and Heat Fluxes. Mon. Wea. Rev., 139, 3781-3797.

Berthelsen, P. A. and Ytrehus, T., 2005. Calculations of stratified wavy two-phase flows in pipes. Int. J. of Multiphase Flow, 31, 571-592.

Biberg, D. 2007. A mathematical model for two-phase statified pipe flow. Multiphase Science and Technology, 19, 1-15.

Blyth, M. G. and Pozrikidis, C., 2004. Effect of inertia on the Marangoni instability of two-layer channel flow, Part II: normal-mode analysis. Journal of Engineering Mathematics 50, 329341.

Charnock, H., 1955. Wind stress over a water surface. Quart. J. Roy. Meteorol. Soc., 81, 639-640.

de Sampaio, P. A. B., Faccini, J. L. H., Su, J., 2008. Modelling of stratified gas-liquid two-phase flow in horizontal circular pipes. Int. J. of Heat and Mass Transfer, 51, 2752-2761.

Danov, K. D., Kralchevsky, P. A. and Ivanov, I.B. 2001. Dynamic Processes in Surfactant Stabilized Emulsions. Chapter 26 in "Encyclopedic Handbook of Emulsion Technology", Sjöblom, J., Ed. (Marcel Dekker: New York, 2001) p. 621-659.

Durbin, P.A., Medic, G., Seo, J.-M., Eaton, J.K., Song, S., 2001. Rough wall modification of two-layer k-ϵ. Journal of Fluids Engineering, Transactions of the ASME 123 (1), 16.

Fakharian, F., 2013. 3D LBM Simulations of Interfaces in Turbulent Multiphase Flow. M.Sc. Thesis, Technical University of Munich and FACE.

Fernando, H. J. S., 1991. Turbulent mixing in stratified fluids. Ann. Rev. Fluid Mech., 23, 455-493.

Fulgosi, M., Lakehal, D., Banerjee, S. and De Angelis, V., 2003. Direct numerical simulation of turbulence in a sheared air-water flow with a deformable interface. J. Fluid Mech., 482, 319-345.

Furtado, K and Skartlien, R., 2010. Derivation and thermodynamics of a lattice Boltzmann model with soluble amphiphilic surfactant. Phys. Rev. E., 81, 0667041-11.

Guo, X. and Shen, L., 2003. Interaction of a deformable free surface with statistically steady homogeneous turbulence. J. Fluid Mech., 658, 33-62.

Lee, R.J. and Saylor, J.R., 2010. The effect of a surfactant monolayer on oxygen transfer across an air/water interface during mixed convection, International Journal of Heat and Mass Transfer 53, 3405-3413.

Lombardi, P., De Angelis, V. and Banerjee, S., 1996. Direct numerical simulation of near-interface turbulence in coupled gas-liquid flow. Phys. Fluids, 8, 1643-1665.

Lugt, H. J. and Ohring, S., 1992. The oblique ascent of a viscous vortex pair toward a free surface. J. Fluid Mech., 236, 461-476.

Ménard, T., Tanguy, S., Berlemont, A., 2007. Coupling level set/VOF/ghost fluid methods: Validation and application to 3D simulation of the primary break-up of a liquid jet. Int. J. of Multiphase Flow, 33, 510-520.

Rein, M., 1998. Turbulent Open-channel Flows: Drop-Generation and Self-Aeration. J. of Hyd. Eng., 1, 98-102.

Sarpkaya, T., 1996. Vorticity, free surface, and surfactants. Annu. Rev. Fluid. Mech., 28, 83-128.

Skartlien, R., Furtado, K., Sollum, E., Meakin, P., Kralova, I., 2011. Lattice-Boltzmann simulations of dynamic interfacial tension due to soluble amphiphilic surfactant. Physica A 390, 2291-2302.

Skartlien, R., Hu, B., Palmer, T.L., Staff, G., Sollum, E., 2014. A statistical model for the average volume fraction profile through the mixing zone in turbulent stratified gas–liquid flow. International Journal of Multiphase Flow 59, 160-172.

Smolentsev, S., and Miraghaie, R., 2005. Study of a free surface in open-channel water flows in the regime from weak to strong turbulence. Int. Journal of Multiphase Flow, 31, 921-939.

Tsai, W-T., 1996. Impact of a surfactant on a turbulent shear layer under the air-sea interface. Journal of Geophysical Research, 101, 28.557-28.568.

ten Cate, A., van Vliet, E., Derksen, J.J., Van den Akker, H.E.A., 2006. Application of spectral forcing in lattice-Boltzmann simulations of homogeneous turbulence. Computers and Fluids, 35, 1239-1251. in stratified flows. Int. J. of Multiphase Flow, 37, 967-976.

Wu, J., Wind-Stress Coefficients over Sea Surface near Neutral Conditions - A Revisit. Journal of Physical Oceanography, 10, 727-740.